ISAR High Resolution Imaging Algorithm Based on Weighted Adaptive Mixed Norm

Qing ZHANG [1], Qianqian CHEN [1], Gang XU [2], Jieru CHI [1]

[1] The College of Electronic Information, Qingdao University, Qingdao, Shandong, China
[2] State Key Laboratory of Millimeter Waves, Southeast University, Nanjing, Jiangsu, China

507542679@qq.com, qqchen@qdu.edu.cn, gangxu@seu.edu.cn, chijieru@qdu.edu.cn

Submitted April 25, 2024 / Accepted August 27, 2024 / Online first October 31, 2024

Abstract. *Based on the sparsity of inverse synthetic aperture radar (ISAR) signal, this paper proposes a high resolution imaging algorithm for ISAR based on weighted adaptive mixed norm. By weighting against $l_{2,0}$ mixed norm term, an improved model of the sparse constraint ISAR signal is proposed. The model effectively distinguishes the signal and noise by adding the weight coefficient, and improves the reconstruction accuracy of the strong scattering center. Meanwhile, the weight coefficients in this improved model can be iteratively updated in each cycle to improve the image reconstruction accuracy. The optimization model takes advantage of $l_{2,0}$ mixed norm to achieve fast convergence in the operation, and adopts conjugate gradient descent method and fast Fourier transform operation in the solution, which simplifies the solving process of the optimization problem and improves the operation efficiency of the algorithm. Simulation data and measured data verify the effectiveness of the proposed method.*

Keywords

Inverse Synthetic Aperture Radar (ISAR), weight coefficient, sparse constraint, regularization coefficient, $l_{2,0}$ mixed norm

1. Introduction

Inverse synthetic aperture radar (ISAR) is an important branch in the development of synthetic aperture radar. Its imaging process is a process in which static radar conducts two-dimensional high resolution imaging including range and azimuth of moving targets [1]. Usually, in ISAR imaging, the high range resolution is obtained by transmitting a wideband signal [2], and the azimuth resolution is achieved by utilizing the rotational motion between the radar and targets. Under long Coherent Processing Interval (CPI) observation, the bigger the angle of target relative to radar, the higher the azimuth resolution [3]. As a result, a two-dimensional ISAR image of the target can be obtained. However, in practical application, due to the mobility characteristics of the ISAR target and the interference of the external environment, the sampling results are not ideal during long CPI observation. In contrast, the short CPI sampling requires a short time [4], and the target movement can be regarded as a smooth movement during observation, but there are also defects of small number of echoes and low resolution of reconstruction image, which is not conducive to subsequent operations. Studying the imaging process of ISAR can find that the main amount of information required in image reconstruction is only provided by strong scattering points, and the number of strong scattering points in the scattering point system is very small, so it can be found that ISAR images have sparsity characteristics [5].

Based on the sparsity of the ISAR signal, many researchers have recently studied the ISAR high resolution imaging algorithms deeply. The ordinary compression sensing (CS) super-resolution imaging algorithm can successfully recover the signal from low dimensional sparse to high dimensional, but under the condition of low signal to noise ratio (SNR), it cannot accurately focus the image due to excessive noise information [6]. To solve this disadvantage, a weighted compression sensing (WCS) imaging algorithm based on CS algorithm is proposed [7]. In this algorithm, the effective signal and noise are effectively distinguished by assigning different weights. So this algorithm effectively improves the problem of poor imaging performance at low signal-to-noise ratio and improves the noise tolerance performance. Although CS and WCS algorithms are able to reconstruct ISAR images under short CPI observation, as these two algorithms need to be optimized and solved by CVX method, they have great challenges in terms of operation complexity and efficiency. The core of ISAR high resolution imaging is the high resolution reconstruction of the target sparse signal obtained by the short aperture sampling [8]. In other words, it is the accurate information recovery of the target sampled by the short CPI in the presence of noise interference. With the continuous improvement of research, a high resolution imaging algorithm based on l_1 norm sparse constraint is proposed [9]. When the observation method is short CPI sampling, the algorithm combines the statistical information of sparse signal and noise collected to derive a method to achieve high resolution reconstruction of target signal under noise

DOI: 10.13164/re.2024.0603

interference by solving an optimization problem with minimum constraint. This algorithm can successfully achieve accurate and efficient recovery of target images in testing. Based on the above algorithm, an adaptive sparse constraint ISAR high resolution imaging algorithm based on $l_{2,0}$ mixed norm, which combines the advantages of l_2 norm and l_0 norm [10]. The sparse constraint optimization model established by this algorithm can realize the adaptive adjustment of the regularization coefficient according to the sparsity of each iteration in the case of any positive SNR, and can determine a relatively stable only a few iteration cycles, thus shorten the running time of the algorithm and improve the solution efficiency.

To improve the accuracy of image reconstruction, we propose an ISAR high resolution imaging algorithm based on the regularization coefficient adaptive adjustment algorithm and the $l_{2,0}$ mixed norm algorithm. The main advantages of the proposed algorithm are

1) In this algorithm, a sparse constraint optimization improved model is established by using the weighted $l_{2,0}$ mixed norm. The model can add different weight coefficients to the strong scattering center [11] and the noise support center according to the signal amplitude. In this way, the target scattering center and the noise support center are treated differently, achieving the purpose of ensuring the original image recovery while suppressing the strong noise.

2) The algorithm introduces an iterative operation to update the weight coefficients related to the amplitude of the signal. With each iteration operation, the reconstruction accuracy of the image improves, leading to more precise weight coefficients. These accurate weight coefficients, in turn, enhance the accuracy of image reconstruction. This iterative process creates a symbiotic relationship between the improvement in weight coefficient accuracy and the enhancement of image reconstruction precision. The operation can effectively improve the accuracy of high resolution image reconstruction.

3) The regularization coefficient can be adjusted adaptively according to the result of each signal iteration

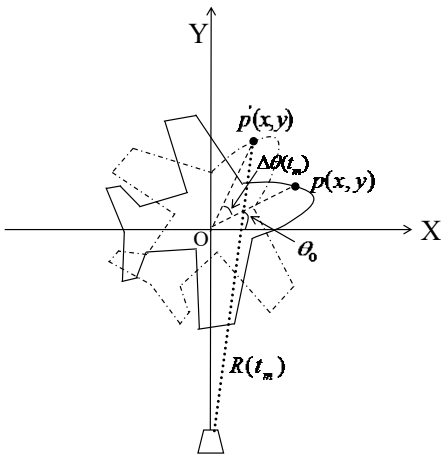

Fig. 1. Rotating signal model.

under different noise. Combining the $l_{2,0}$ mixed norm and conjugate gradient descent method ensures the operation efficiency, so that the algorithm has better effectiveness and superiority in the operation.

The paper is organized as follows. In Sec. 2, the theoretical knowledge of the ISAR imaging signal model is briefly introduced. In Sec. 3, the optimization model based on the weighted adaptive mixed norm is proposed and the solution algorithm is given to reconstruct the target signal by authors. Section 4 presents ISAR imaging results of simulated and measured data. Section 5 provides the conclusion and possible future directions.

2. ISAR Imaging Signal Model

After the radar acquired the target echoes, the imaging model is drawn in a two-dimensional plane for simplicity, where the Y axis and X axis represent the distance and azimuth direction respectively. After the envelope alignment and initial phase correction, the simplified ISAR signal model is obtained, as shown in Fig. 1.

For the simplified rotation signal model, the angle change of the target relative to the radar in the case of short CPI can be approximated as

$$\Delta\theta\left(t_m\right) \approx \omega t_m \tag{1}$$

where t_m is slow time, $0 \le t_m \le T$, T is coherent processing time length; ω is the rotational angular velocity of the target. Due to the size of the reflected target is much smaller than the distance between the target and the radar, after the motion compensation and phase correction of the echo data, at which time the distance between the scattering point $p(x,y)$ on the target and the radar can be approximated as

$$R\left(t_m\right) = R_0 + y\cos\left(\Delta\theta\left(t_m\right)\right) + x\sin\left(\Delta\theta\left(t_m\right)\right) \tag{2}$$

where R_0 represents the distance between radar and target rotation center O. In a short CPI observation, Equation (1) can substitute the target rotation angle $\Delta\theta(t_m)$, yielding an approximate formula for the distance between the target scattering point and the radar

$$R\left(t_m\right) = R_0 + y + x\sin\left(\omega t_m\right). \tag{3}$$

Generally, the radar transmitting signal is linear frequency modulation signal

$$s(t_{\mathrm{r}}) = \mathrm{rect}\left[\frac{t_{\mathrm{r}}}{T_{\mathrm{p}}}\right] \cdot \exp\left[2\pi\left(f_{\mathrm{c}}t_{\mathrm{r}} + \frac{\alpha}{2}t_{\mathrm{r}}^2\right)\right] \tag{4}$$

where t_{r} represents the sampling fast time; T_{p} represents pulse width; f_{c} represents the carrier frequency; α represents the modulation frequency; rect[·] represents a window function. When the target size is large, the target movement may produce the Migration Though Resolution Cell (MTRC) situation, which needs to be compensated

[12]. The echo signal after MTRC compensation is pulse compressed to obtain

$$s(t_{\mathrm{r}},t_m)\approx\beta_p\cdot\mathrm{rect}\left[\frac{t_m}{T}\right]\cdot\mathrm{sinc}\left[T_{\mathrm{p}}\alpha\left(t_{\mathrm{r}}-\frac{2(r_0+y)}{C}\right)\right]\cdot \exp\left[-\mathrm{j}4\pi\frac{r(t_m)}{\gamma}\right] \tag{5}$$

where β_p represents the target scattering coefficient of the scattering point p, which can be regarded as a constant when the rotation angle of the target is very small; γ is the radar transmitting signal wavelength; C is the speed of light. Under considering noise, when there are N scattering points in the range cell with a distance of r_0+y, the echo signal of this range cell is

$$s(t_m)=\sum_{p=1}^{N}B_p\cdot\mathrm{rect}\left[\frac{t_m}{T}\right]\cdot\exp(-2\pi\mathrm{j}f_p t_m)+n \tag{6}$$

where B_p represents the scattering coefficient of the scattering point p at the azimuth moment t_m, and $B_p=\beta_p\cdot\exp\left(-4\pi\mathrm{j}\frac{r_0+y}{\gamma}\right)$. f_p represents the Doppler frequency of the scattering point p, and $f_p=2\omega x/\gamma$; n is additive noise. To obtain the pixel distribution of the image domain, the orientation Fourier transform of (6) is required

$$s(f_d)=\sum_{p=1}^{N}B_p\cdot\mathrm{sinc}[T(f_d-f_p)]+n. \tag{7}$$

3. ISAR High Resolution Imaging Based on Weighted Adaptive Mixed Norm

3.1 ISAR Optimization Imaging Model Based on Weighted Adaptive $l_{2,0}$ Mixed Norm Sparse Constraint

In the case of short CPI sampling observation, the target movement can be regarded as a smooth motion, and the sampled signal echoes are less affected by noise and more stable. Based on the sparsity of the ISAR signal, the signal model shown in (6) can be discretized. On the short CPI sampling observation, if there are $\hat{M}$ effective pulses within each range cell, the ISAR echo signal is expressed as

$$\mathbf{S}=\mathbf{F}\mathbf{X}+\boldsymbol{\varepsilon} \tag{8}$$

where $\mathbf{S}$ represents the ISAR echo signal on the short CPI observation, whose size is $\hat{M}\times N$, $\hat{M}$ is the total number of sampling pulses, N is the sampling points of range profile. Under the short CPI observation, the small number of echo pulses is obtained. To obtain azimuthal high resolution, long CPI observations are required. We need an algorithm to achieve the reconstruction of the full-aperture images by the small number of echo pulses. $\mathbf{X}$ represents the target image to be reconstructed of size $M\times N$, and M is the number of pulses emitted by the signal under the full-aperture observation. In the simulation and measured experiments in this paper, the number of pulses corresponding to high resolution is 256, that is, the number of full aperture pulses is set to 256. $\boldsymbol{\varepsilon}$ represents an additive complex noise matrix, whose dimension is equivalent to $\mathbf{S}$; $\mathbf{F}$ represents a partial Fourier transform matrix with a size of $\hat{M}\times M$, and $\hat{M}\ll M$.

$$\mathbf{F}=\begin{bmatrix}1 & 1 & \cdots & 1\\ 1 & \omega & \cdots & \omega^{M-1}\\ \vdots & \vdots & \ddots & \vdots\\ 1 & \omega^{\hat{M}-1} & \cdots & \omega^{(\hat{M}-1)(M-1)}\end{bmatrix}_{\hat{M}\times M} \tag{9}$$

where $\omega=\exp\left(-\mathrm{j}\frac{2\pi}{M}\right)$.

In (8), the solution of the target matrix is to accurately recover the full aperture of the target signal in the presence of noise interference. In the adaptive sparse constraint ISAR high resolution imaging algorithm based on mixed norm, signal and noise in the echo are treated equally, leading to the inability to achieve high resolution reconstruction of images under strong noise. To more accurately distinguish between the effective signal and the noise [13], different weight coefficients are added to the signal and the noise in the echo according to the amplitude. Meanwhile, combined with the adaptive regularization coefficient [14], we propose an ISAR high resolution imaging model based on the weighted adaptive mixed norm sparse constraint as

$$\hat{\mathbf{X}}=\arg\min\left\{\left\|\mathbf{S}-\mathbf{F}\mathbf{X}\right\|_2^2+\tilde{\lambda}\tilde{\mathbf{W}}\sum_{m=1}^{M}\left(1-\exp\left(-\beta\left\|\mathbf{X}_m\right\|_2\right)\right)\right\} \tag{10}$$

where $\tilde{\lambda}$ represents the adaptive regularization coefficient. In the case of uncertain SNR, λ is adjusted according to the noise variance and the Laplace coefficient to balance the relationship between image sparsity and estimation error [10]. $\tilde{\mathbf{W}}$ is the diagonal matrix of the weight coefficient, and each cycle can be updated iteratively.

The relationship between the weight coefficient [15] and the signal amplitude can be expressed as

$$w_n=\frac{1}{\left|\mathbf{X}_{\mathrm{f}}(n)\right|+\delta} \tag{11}$$

where $\mathbf{X}_{\mathrm{f}}$ is obtained from Fourier transform of the matrix $\mathbf{X}$, δ represents a small value constant.

In order to ensure the accuracy of the weight coefficient, the value of the weight coefficient needs to change after each cycle, so an iterative algorithm is introduced. During the iteration process, the weight coefficient is updated according to (11), making the weight matrix more accurate and improving constantly the imaging resolution. The weight coefficient iteration formula is

$$w_n^{i+1} = \frac{1}{\left|\mathbf{X}_{\mathrm{f}}^{i}(n)\right| + \delta} \tag{12}$$

where $\mathbf{X}_{\mathrm{f}}^{i}(n)$ represents the n element of the image vector after the i reconstruction; w_n^{i+1} represents the weight coefficient corresponding to the n element of the image vector during the $(i+1)$ reconstruction, and the diagonal matrix composed of w_n obtained by the last reconstruction is $\mathbf{W}$.

3.2 Solution of Improved ISAR Imaging Model Based on the Weighted Adaptive Mixed Norm

The quasi-Newton algorithm [16] solves the optimization problem shown in (10). In order to avoid the non-differentiable problem in the process of solving the mixed norm, a minimal non-negative value φ is used to approximate (10)

$$\begin{aligned}\hat{\mathbf{X}} &= \arg\min \left\{ \left\|\mathbf{S}-\mathbf{F}\mathbf{X}\right\|_2^2 + \tilde{\lambda}\tilde{\mathbf{W}}\sum_{m=1}^{M}\left(1-\exp\left(-\beta\sqrt{\sum_{n=1}^{N}\left|x_{mn}\right|^2+\varphi}\right)\right)\right\} \\ &= \arg\min\left(f\left(\mathbf{X}\right)\right)\end{aligned} \tag{13}$$

where $\sqrt{\sum_{n=1}^{N}\left|x_{mn}\right|^2+\varphi}$ is the approximation of $\|\mathbf{X}_m\|_2$ in (10).

The conjugate gradient function of $f(\mathbf{X})$ is

$$\begin{aligned}\nabla f(\mathbf{X}) &= 2\mathbf{F}^{\mathrm{H}}\mathbf{F}\mathbf{X} + \tilde{\lambda}\tilde{\mathbf{W}}\boldsymbol{\Lambda}(\mathbf{X})\mathbf{X} - 2\mathbf{F}^{\mathrm{H}}\mathbf{S} \\ &= \mathbf{H}(\mathbf{X})\mathbf{X} - 2\mathbf{F}^{\mathrm{H}}\mathbf{S}.\end{aligned} \tag{14}$$

The Hessian matrix $\mathbf{H}(\mathbf{X})$ is

$$\mathbf{H}(X) = 2\mathbf{F}^{\mathrm{H}}\mathbf{F} + \tilde{\lambda}\tilde{\mathbf{W}}\boldsymbol{\Lambda}(\mathbf{X}) \tag{15}$$

where λ in $\mathbf{H}(X)$ is updated with each iteration; $\boldsymbol{\Lambda}(X)$ is a diagonal matrix, and the expression is

$$\boldsymbol{\Lambda}(\mathbf{X}) = \left(\operatorname{diag}\left[\beta\frac{\exp\left(-\beta\sqrt{\left|\mathbf{X}_m\right|^2+\varphi}\right)}{\sqrt{\left|\mathbf{X}_m\right|^2+\varphi}}\right]\right)_{m\times m}. \tag{16}$$

Because the Hessian matrix contains the objective function to be solved, it can be solved directly by iterative method

$$\bar{\mathbf{X}}^{n+1} = \left[\mathbf{H}\left(\bar{\mathbf{X}}^{n}\right)\right]^{-1}\mathbf{F}^{\mathrm{H}}\mathbf{S} \tag{17}$$

where $\bar{\mathbf{X}}^{n}$ represents the result of the n iteration of the objective function $\mathbf{X}$; $[\cdot]^{-1}$ represents the matrix inverse operation. The convergence threshold is set, and when the convergence condition of the target function satisfies $\left\|\bar{\mathbf{X}}^{n+1}-\bar{\mathbf{X}}^{n}\right\|_2^2 \Big/ \left\|\bar{\mathbf{X}}^{n}\right\|_2^2 \le \rho$, the iteration cycle ends and the final result is obtained.

In (17), the inversion operation of Hessian matrix is realized by the conjugate gradient descent method in the algorithm, which avoids the huge amount of operation generated by the inversion operation of Hessian matrix and improves the operation efficiency [17]. In addition, the fast Fourier transform and its inverse transform operation [18] are used to solve the problem of the Fourier dictionary matrix and the reconstructed target product operation in (14), which also reduces the amount of operation in the execution process of the algorithm and improves the operation speed.

For clarity, we give the detailed flow of solution of improved ISAR imaging model based on the weighted adaptive mixed norm as follows. First, in the case of short CPI observation, we obtain a small number of echo pulses with the number of pulses of $\hat{M}$ and the pulses number of the full-aperture image is M. We use matched filter or the dechirp method for pulse compression in the simulation. To be more realistic, complex Gaussian noise is added into the signal. After the compensation of translational motion, the range-oriented imaging result of simulation data by $\hat{M}$ echo pulses is obtained. Next, the range-oriented image is processed by the high-resolution algorithm proposed in this paper. The following is an introduction to the high-resolution algorithm flow. After the parameter initialization, Hessian function $\mathbf{H}(\mathbf{X})$ is constructed. Then we use conjugate gradient descent method to obtain optimal solution $\hat{\mathbf{X}}$. Terminate on convergence or when attains a specified maximum number of iterations max. Otherwise, update $\boldsymbol{X}_{\mathrm{f}}$, regularization coefficient $\tilde{\lambda}$ and weight coefficient w_n, and continue to iterate. Finally, the reconstructed images with M pulses are obtained.

4. Verification of Experimental Data

In this paper, an improved ISAR imaging model based on the weighted adaptive mixed norm model is established and that is an improvement of the optimization imaging model based on mixed norm sparse constraint [10]. Simulation data and measured data are used to verify the imaging results of the proposed algorithm, and compare the imaging results of the proposed algorithm with the algorithm based on the $l_{2,0}$ mixed norm and the ISAR high-resolution imaging algorithm based on the l_1 norm in the case of different numbers of echo pulses and SNRs [19]. The above algorithms are based on the optimization imaging model with norm sparse constraint, and all obtain the objective function employ the maximum a posteriori (MAP) estimator.

In order to verify the reconstruction performance of the algorithm, the paper tests the algorithm through the MATLAB 2020a processing platform and run on a working

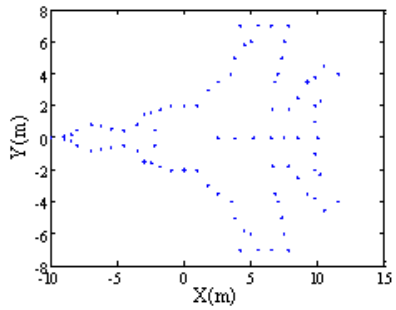

Fig. 2. Aircraft scatter point model.

Radar carrier frequency	9.15 GHz
Radial velocity	100 m/s
Signal bandwidth	400 MHz
Pulse repetition frequency	125 Hz
Rotational angular velocity	0.0216 rad/s
Range direction resolution	0.375 m

Tab. 1. Main simulation parameters of the radar system.

station with Intel(R) Core(TM) i7-8565U CPU @ 1.80 GHz 1.99 GHz and 16.0 GB RAM.

In the simulation experiments, the target model is shown in Fig. 2. The relevant parameters of the radar used are shown in Tab. 1.

The distance between the rotation center of the radar and the target is 10 000 m, and the amplitude of each scattering point is 1. Under the short CPI observation, 64 echoes are taken for processing, and the super resolution image with a length of 256 is reconstructed. The iteration threshold is $\rho = 10^{-4}$, the number of iterations is set to 500, and the constant $\varphi = 10^{-6}$.

In the case of short CPI observation, we obtain 64 echo pulses and use matched filter for pulse compression in the simulation. The range-oriented imaging result obtained after the compensation of translational motion is shown in Fig. 3. Figure 4 shows the result of the simulation data processed with traditional Range-Doppler (RD) algorithm, and Figure 5 shows the full-aperture image of the 256 pulses about the simulation data.

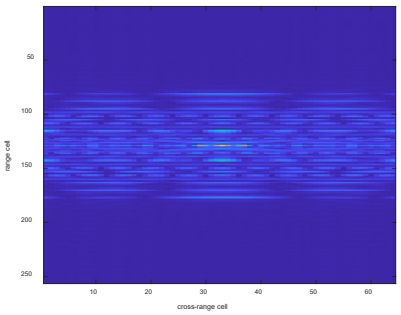

Fig. 3. Range-oriented imaging result of simulation data by 64 echo pulses.

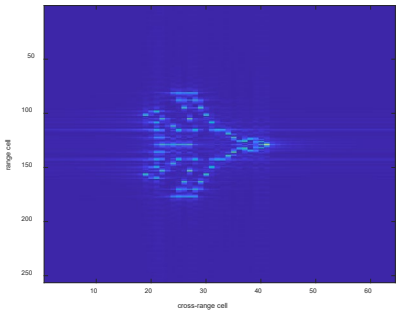

Fig. 4. Imaging result of RD algorithm by 64 echo pulses.

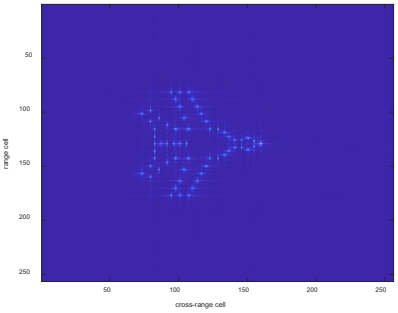

Fig. 5. Full-aperture image of the 256 pulses.

To further evaluate the image quality, the mean square error (MSE) index is introduced to quantitatively evaluate the imaging results [20]. MSE is an indicator used to calculate the accuracy of image recovery, which is defined as shown in (18). The smaller the value, the higher the accuracy of image recovery, that is, the better the reconstruction effect

$$\mathrm{MSE} = \frac{\left\|\mathbf{X} - \hat{\mathbf{X}}\right\|_F}{\left\|\mathbf{X}\right\|_F} \tag{18}$$

where $\mathbf{X}$ is the full-aperture image of the 256 pulses and $\hat{\mathbf{X}}$ is the reconstructed image.

To verify the effectiveness of the algorithm proposed in this paper under different numbers of echo pulses, we choose two other algorithms to compare with the algorithm proposed in this paper under small amount of echo pulses. Under the short CPI observation, through 50 experiments with numbers of echo pulses ranging from 32 to 64 in step of 4, and the super-resolution image with the length of 256 is reconstructed.

Under different numbers of echo pulses, three algorithms are used for operation. In Fig. 6, the blue broken line is the MSE obtained by the algorithm proposed in this paper, the red line is the MSE obtained by the algorithm based on the $l_{2,0}$ mixed norm, and the yellow line is the MSE obtained by the algorithm based on the l_1 norm. It can be seen that there is little difference in MSE between the ISAR high resolution imaging algorithm based on the l_1 norm and the one based on the $l_{2,0}$ mixed norm. However, the imaging efficiency of algorithm based on the $l_{2,0}$ mixed norm is higher than that of the l_1 norm[10]. As can also be

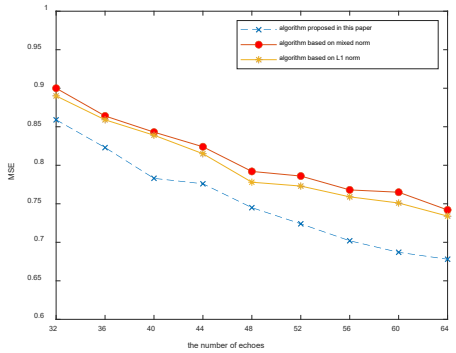

Fig. 6. Curve of MSE with the number of echo pulses.

seen from Fig. 6, the MSE of the algorithm proposed in this paper is smaller than the previous algorithms based on the norm at different numbers of echoes. In summary, the algorithm based on the $l_{2,0}$ mixed norm is an improvement of the algorithm based on the l_1 norm and the algorithm proposed in the paper is an improvement of the algorithm based on the $l_{2,0}$ mixed norm. Therefore, in the following comparison of the imaging results, we only present the imaging results of algorithm based on the $l_{2,0}$ mixed norm and the one proposed in the paper.

To verify the effectiveness of the algorithm proposed in this paper in the natural environment, different SNRs (5 dB, 10 dB, 20 dB) are set by adding Gaussian white noise into the echo signal. In the case of different SNRs, the results of processing the simulation data using the proposed algorithm and the imaging algorithm based on the $l_{2,0}$ mixed norm [10] are shown in Figs. 7–12.

Figures 7, 9 and 11 in turn represent the imaging results obtained according to the imaging algorithm based on the $l_{2,0}$ mixed norm at SNRs of 5 dB, 10 dB and 20 dB. Figures 8, 10 and 12 in turn represent the imaging results obtained according to the proposed algorithm at SNRs of 5 dB, 10 dB and 20 dB.

In Fig. 13, Gaussian white noise is added to the simulation data images and the SNR ranges from 2 dB to 20 dB. The interval between the data points is 2 dB. The blue broken line is the MSE obtained by the algorithm proposed in this paper, the red line is the MSE obtained by the algorithm based on the $l_{2,0}$ mixed norm and the yellow line is the MSE obtained by the algorithm based on the l_1 norm.

As can be seen from Fig. 13, the MSE obtained by the algorithm in this paper is smaller than the MSE obtained based on the l_1 norm and the $l_{2,0}$ mixed norm imaging algorithm. It can be found that with the decrease of the SNR, the MSE difference of the algorithm in this paper and the other two algorithms based on the norm increases. In other words, the greater the noise, the more obvious the improvement effect, and the higher the image reconstruction accuracy. Combined Figs. 6 and 13 can be found that the reconstruction accuracy based on the algorithm proposed in the paper is higher than the ISAR high resolution imaging algorithm based on the l_1 norm and based on the $l_{2,0}$ mixed norm in the case of different number of samples and SNRs.

To further verify the effectiveness of the algorithm proposed in this paper, a set of measured data from the target aircraft Yak-42 is used, and the aircraft model is shown in Fig. 14.

The measured data is the echo data of the Yak-42 aircraft recorded by the C-band experimental system and the

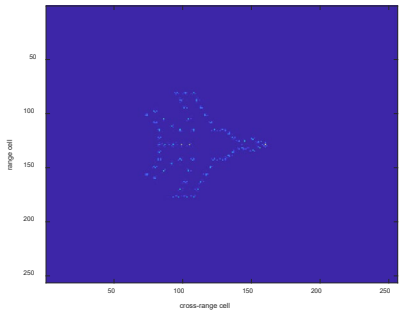

Fig. 7. Imaging result of mixed norm at SNR = 5 dB.

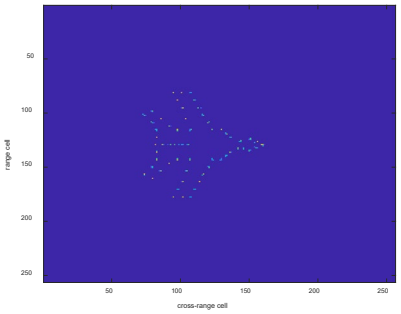

Fig. 8. Imaging result of the algorithm proposed in this paper at SNR = 5 dB.

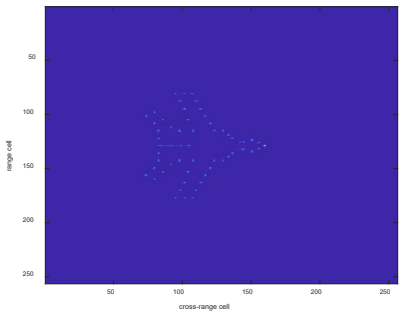

Fig. 9. Imaging result of mixed norm at SNR = 10 dB.

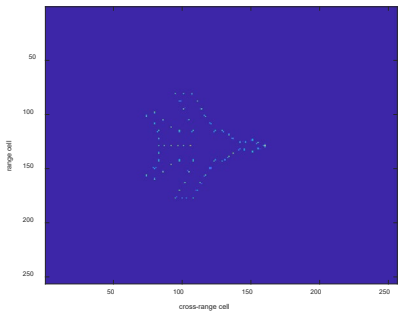

Fig. 10. Imaging result of the algorithm proposed in this paper at SNR = 10 dB.

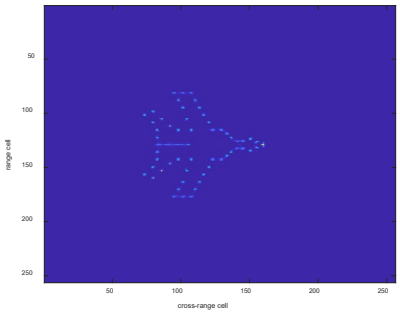

Fig. 11. Imaging result of mixed norm at SNR = 20 dB.

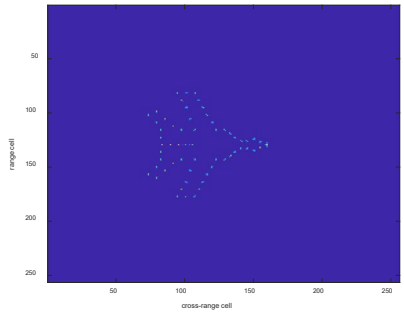

Fig. 12. Imaging result of algorithm proposed in this paper at SNR = 20 dB.

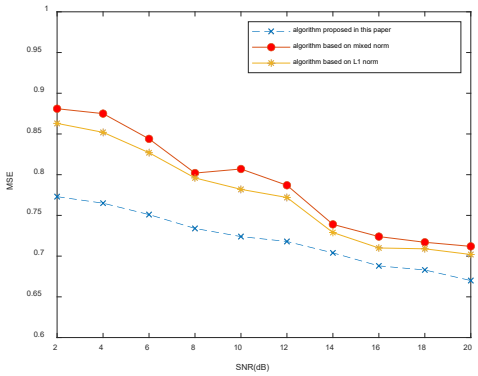

Fig. 13. Curve of MSE with different SNR.

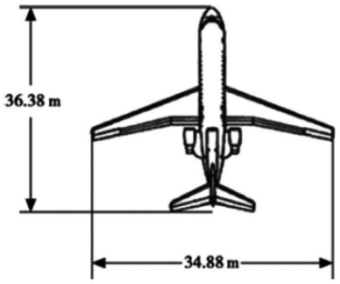

Fig. 14. Yak-42 model.

main radar system parameters are shown in Tab. 2. The imaging results of the algorithm proposed in this paper from the simulation data show that the improvement effect is better at a low SNR. Therefore, for the imaging results of the measured data at a low SNR, we take the imaging results obtained at 5 dB as examples to verify the effectiveness of the algorithm proposed in this paper. The test parameter setting and the data processing amount are the same as the simulation data processing.

In the case of short CPI observation, we obtain 64 echo pulses and use the dechirp method for pulse compression in the simulation. The range-oriented imaging result obtained after range-alignment and phase-adjustment is shown in Fig. 15. The imaging result obtained by the conventional ISAR imaging algorithm is shown in Fig. 16, and Figure 17 represents the full-aperture image of the 256 pulses about the measured data.

Radar carrier frequency	5.52 GHz
Transmission signal bandwidth	400 MHz
Sampling frequency	10 MHz
Range direction resolution	0.375 m
Pulse repetition frequency	100 Hz

Tab. 2. Main measured parameters of the radar system.

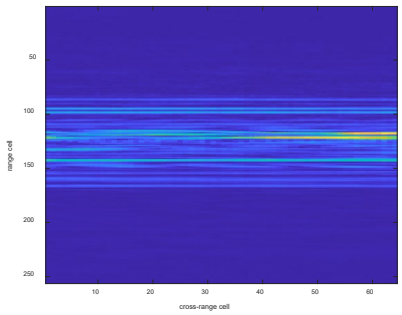

Fig. 15. Range-oriented imaging result of measured data by 64 echo pulses.

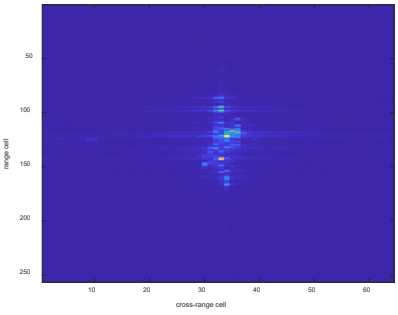

Fig. 16. Imaging result of traditional RD algorithm by 64 echo pulses.

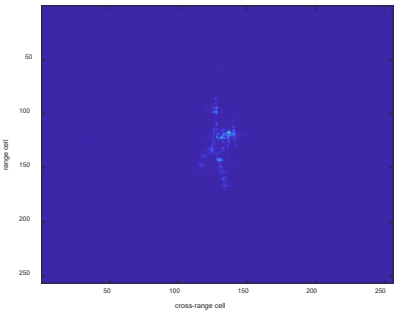

Fig. 17. Full-aperture image of the 256 pulses.

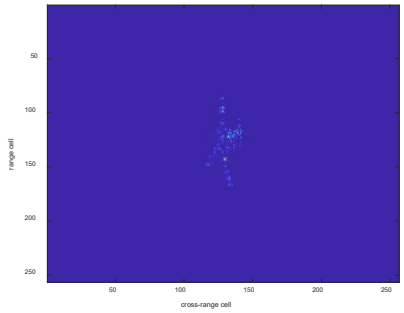

Fig. 18. Imaging result of mixed norm at SNR = 5 dB.

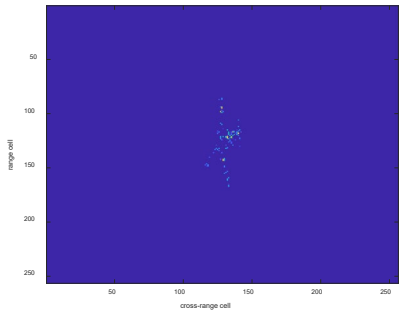

Fig. 19. Imaging result of the algorithm proposed in this paper at SNR = 5 dB.

Figure 18 illustrates the imaging result obtained according to the imaging algorithm based on the $l_{2,0}$ mixed norm [10] at a SNR of 5 dB. Meanwhile, Figure 19 depicts the imaging result obtained with the proposed algorithm at a SNR of 5 dB.

Due to the addition of weight coefficient and the introduction of the iterative algorithm for updating the weight coefficients in the proposed algorithm in this paper, the reconstructed images of the two algorithms are different to some extent. Therefore, the MSE is also different. The image reconstruction accuracy of the algorithm proposed in this paper is higher than that of the original algorithm based on mixed norm under the measured data. At a SNR of 5 dB, the MSE of algorithm based on mixed norm is 1.137, and the MSE of the algorithm proposed in this paper is 1.035. It can be seen that the MSE obtained by the algorithm proposed in this paper is smaller than that obtained by the original algorithm based on mixed norm. The effectiveness of the algorithm proposed in this paper is proved.

5. Conclusion

In this paper, based on the sparsity of ISAR images and combined with the adaptive adjustment algorithm of regularization coefficient we propose an improved sparse constrained ISAR signal model based on the weighted mixed norm. The model realizes the effective distinction of the strong scattering center and the noise support area by weighting $l_{2,0}$, and the weight coefficient can be updated according to the result of each iteration, thus ensuring the accuracy of image reconstruction. And then, the model avoids the complex process of repeated attempts of the regularization coefficient, takes advantage of the fast convergence rate of the $l_{2,0}$ mixed norm, combines the conjugate gradient algorithm and the fast Fourier transform, to effectively improve the operation efficiency. Future work includes: extending the proposed algorithm to achieve high quality ISAR 3D imaging under short CPI; combining the proposed algorithm with machine learning to improve the algorithm adaptability.

Acknowledgments

During the completion of the paper, the authors would like to especially thank the editors and anonymous reviewers for their professional guidance and selfless help. The meticulous work of the editors and the rigor of the reviewers make the paper more perfect in structure and content. The authors sincerely appreciate their contributions and look forward to more opportunities for cooperation in the future. This work was supported by the Natural Science Foundation of Shandong Province under Grant ZR2021MF025.

References

[1] ZENG, C. Z., ZHU, W. G., JIA, X. Bistatic inverse synthetic aperture radar imaging method for the high-speed motion target. *Journal of Applied Remote Sensing*, 2018, vol. 12, no. 4, p. 1–17. DOI: 10.1117/1.jrs.12.045012

[2] YANG, S., LI, S., FAN, H., et al. High resolution ISAR imaging of maneuvering targets based on azimuth adaptive partitioning and compensation function estimation. *IEEE Transactions on Geoscience and Remote Sensing*, 2023, vol. 61, p. 1–15. DOI: 10.1109/TGRS.2023.3334770

[3] ZHOU, P., ZHANG, G., YANG, W. A review of ISAR imaging technology. In *2020 IEEE International Conference on Information Technology, Big Data and Artificial Intelligence (ICIBA)*. Chongqing (China), 2020, p. 664–668. DOI: 10.1109/ICIBA50161.2020.9277180

[4] NEPAL, R., CAI, J., YAN, Z. Micro-Doppler radar signature identification within wind turbine clutter based on short-CPI airborne radar observations. *IET Radar, Sonar and Navigation*, 2015, vol. 9, no. 9, p. 1268–1275. DOI: 10.1049/iet-rsn.2015.0111

[5] ZHU, H. S., HU, W. H., GUO, B. F., et al. A bistatic inverse synthetic aperture radar sparse aperture high-resolution imaging algorithm with migration compensation. *IET Radar, Sonar and Navigation*, 2022, vol. 16, no. 12, p. 1949–1962. DOI: 10.1049/rsn2.12309

[6] WU, K., CUI, W., XU, X. Superresolution radar imaging via peak search and compressed sensing. *IEEE Geoscience and Remote Sensing Letters*, 2022, vol. 19, p. 1–5. DOI: 10.1109/LGRS.2022.3184067

[7] XU, G., ZHANG, B. J., CHEN, J. L., et al. Sparse inverse synthetic aperture radar imaging using structured low-rank method. *IEEE Transactions on Geoscience and Remote Sensing*, 2022, vol. 60, p. 1–12. DOI: 10.1109/TGRS.2021.3118083

[8] JI, B., ZHAO, B., WANG, Y., et al. SA-ISAR imaging algorithm based on the gradient signal recovery method. *The Journal of Engineering*, 2019, no. 20, p. 6577–6581. DOI: 10.1049/joe.2019.0284

[9] CHEN, Q. Q., XU, G., ZHANG, L., et al. Three-dimensional interferometric inverse synthetic aperture radar imaging with limited pulses by exploiting joint sparsity. *IET Radar, Sonar and Navigation*, 2015, vol. 9, no. 6, p. 692–701. DOI: 10.1049/iet-rsn.2014.0275

[10] SONG, D. Y., CHEN, Q. Q., LI, K. Z. An adaptive sparse constraint ISAR high resolution imaging algorithm based on mixed norm. *Radioengineering*, 2022, vol. 31, no. 4, p. 477–485. DOI: 10.13164/re.2022.0477

[11] CHENG, P., CHEN, W., CHENG, J., et al. A fast ISAR imaging method based on strategy weighted CAMP algorithm. *IEEE Sensors Journal*, 2022, vol. 22, no. 17, p. 17022–17030. DOI: 10.1109/JSEN.2022.3192534

[12] CHEN, R., JIANG, Y., LIU, Z., et al. A novel spaceborne ISAR imaging approach for space target with high-order translational motion compensation and spatial variant MTRC correction. *International Journal of Remote Sensing*, 2023, vol. 44, no. 21, p. 6549–6578. DOI: 10.1080/01431161.2023.2272600

[13] CHEN, J. Y., XU, Z. H., XIAO, S. P. Irregular subarray design strategy based on weighted L1 norm iterative convex optimization. *IEEE Antennas and Wireless Propagation Letters*, 2022, vol. 21, no. 2, p. 376–380. DOI: 10.1109/LAWP.2021.3132001

[14] XU, Z. B., CHANG, X. Y., XU, F. M., et al. L1/2 regularization: A thresholding representation theory and a fast solver. *IEEE Transactions on Neural Networks and Learning Systems*, 2012, vol. 23, no. 7, p. 1013–1027. DOI: 10.1109/TNNLS.2012.2197412

[15] CANDES, E. J., WAKIN, M. B., BOYD, S. P. Enhancing sparsity by reweighted l_1 minimization. *Journal of Fourier Analysis and Applications*, 2008, vol. 14, no. 5-6, p. 877–905. DOI: 10.1007/s00041-008-9045-x

[16] ZHANG, W. T., LOU, S. T., FENG, D. Z. Adaptive quasi-Newton algorithm for source extraction via CCA approach. *IEEE Transactions on Neural Networks and Learning Systems*, 2014, vol. 25, no. 4, p. 677–689. DOI: 10.1109/TNNLS.2013.2280285

[17] VAN DER HEIDE, O., SBRIZZI, A., VAN DER BERG, C. A. T. Accelerated MR-STAT reconstructions using sparse Hessian approximations. *IEEE Transactions on Medical Imaging*, 2020, vol. 39, no. 11, p. 3737–3748. DOI: 10.1109/TMI.2020.3003893

[18] PONOMAREV, A., PONOMAREVA, O., SMIRNOVA, N. Evolution of one-dimensional and two-dimensional discrete Fourier transform. In *24th International Conference on Digital Signal Processing and its Applications (DSPA)*. Moscow (Russian Federation), 2022, p. 1–6. DOI: 10.1109/DSPA53304.2022.9790768

[19] RONG, J., WANG, Y., HAN, T. Iterative optimization-based ISAR imaging with sparse aperture and its application in interferometric ISAR imaging. *IEEE Sensors Journal*, 2019, vol. 19, no. 19, p. 8681–8693. DOI: 10.1109/JSEN.2019.2923447

[20] WANG, Z. J., BADIU, M. A., COON, J. P. On the value of information and mean squared error for noisy Gaussian models. *IEEE Communications Letters*, 2022, vol. 26, no. 9, p. 2023–2026. DOI: 10.1109/LCOMM.2022.3188368

[21] LI, D., ZHAN, M. Y., LIU, H. Q., et al. A robust translational motion compensation method for ISAR imaging based on keystone transform and fractional Fourier transform under low SNR environment. *IEEE Transactions on Aerospace and Electronic Systems*, 2017, vol. 53, no. 5, p. 2140–2156. DOI: 10.1109/TAES.2017.2683599

About the Authors ...

Qing ZHANG was born in 2001. She received her B.S. degree from the Qingdao University, in 2023, where she is currently pursuing the MA.Eng. degree with the College of Electronic Information, Qingdao University. Her research interests include radar signal imaging and target recognition.

Qianqian CHEN (corresponding author) was born in 1985. She received her Ph.D. degree in Signal and Information Processing from Xidian University, Xi'an, China, in 2015. She is an Assistant Professor at the Department of Electronic Engineering, Qingdao University. From 2018 to 2019, she was a visiting scholar at the Department of Automatic Control and Systems Engineering, University of Sheffield, UK. Her major research interests are SAR and ISAR imaging.

Gang XU was born in 1987. He received the B.S. and Ph.D. degrees in Electrical Engineering from Xidian University, Xi'an, China, in 2009 and 2015, respectively. From 2015 to 2016, he was a full-time Postdoctoral Research Fellow at the School of Electrical and Electronic Engineering, Nanyang Technological University, Singapore. He is currently a Full Professor at the State Key Laboratory of Millimeter Waves, School of Information Science and Engineering, Southeast University, Nanjing, China. His research interests include synthetic aperture radar (SAR)/inverse SAR (ISAR) imaging and millimeter-wave radar.

Jieru CHI was born in 1970. She received the B.Sc. degree in Automation and M.Sc. degree in Control Science and Engineering from Shandong University, Jinan, China, in 1992 and 1995, and the Ph.D. degree from the Institute of Complexity Science, Qingdao University, in 2019. She is currently a Professor with the College of Electronics and Information, Qingdao University. Her current research interests include artificial intelligence, and intelligent information processing.